

Using anti-squeezed Schrödinger cat states for detection of a given phase shift

V. L. Gorshenin*

Russian Quantum Center, Skolkovo 121205, Russia and
Moscow Institute of Physics and Technology, 141700 Dolgoprudny, Russia

K. D. Dyadkin and S. D. Chikalkin

Russian Quantum Center, Skolkovo 121205, Russia

We propose to use the antisqueezing-enhanced non-Gaussian Schrödinger cat quantum states of the probing light for the task of detection of a given phase shift in optical interferometers. We show that the antisqueezing allows to increase the robustness of the setup to optical losses. We find the optimal degrees of the antisqueezing for experimentally achievable values of the Schrödinger cat amplitude and the optical losses and compare the resulting sensitivity with the one provided by the Gaussian squeezed states.

I. INTRODUCTION

At a fundamental level, the phase sensitivity of an interferometer is limited by quantum fluctuations of the probe field and therefore depends on the probe's quantum state; see, e.g., Refs. [1, 2]. In particular, for a Gaussian coherent squeezed state, the phase estimation can reach the following value [3]:

$$\Delta\phi_{\text{SQZ}} = \frac{e^{-r}}{2\sqrt{N}}. \quad (1)$$

where N is the mean number of photons passing through the phase shifting object(s) and r is the logarithmic squeeze parameter (it is assumed here that the squeezing is not very strong, $e^{2r} \ll N$).

One may also consider “truly quantum” states, characterized by Wigner quasiprobability functions [4] with a non-Gaussian shape. Their potential metrological utility has been investigated extensively [5–13]; see also review [14]). Overall, these studies suggest that, for phase estimation with no prior information about the phase, non-Gaussian probes offer no substantial advantage. Moreover, Refs. [15, 16] showed that optimal sensitivity can be attained using comparatively simple, experimentally accessible Gaussian states.

In contrast, non-Gaussian states can be highly effective for another important interferometric task: binary discrimination between two known phase shifts [17]. For example, one may wish to discriminate between two dielectrics with known, slightly different refractive indices while depositing less optical energy than would be required when using a coherent state of light. This low-energy regime is particularly attractive for interrogating biological specimens that can be damaged by intense illumination [18, 19]. Without loss of generality, one may set one of the two hypothesis to correspond to zero phase shift, so that the task reduces to detecting the presence of a specified phase shift.

Note that the general problem of detection an unknown displacement along an unknown axis using of non-Gaussian states was considered in Ref. [20].

Note also that “unambiguous state discrimination” also refers to an alternative framework introduced in Ref. [21]; see also Refs. [22, 23] and the references therein. In this setting, two nonorthogonal states can be discriminated without any error but the protocol succeeds only with some probability $P_D < 1$ and produces in the rest of the cases. In many applications, such inconclusive events are equivalent to errors.

A Schrödinger-cat (SC) state is a pure state defined as a superposition of two coherent states [24]. The use of SC states has been proposed for quantum computing [25–29], quantum cryptography [30], and quantum error correction [31].

In Ref. [32], we proposed to use the even Schrödinger cat (SC) states of the form

$$|\Psi_0\rangle = \frac{1}{\sqrt{K}}(|\alpha\rangle + |-\alpha\rangle) \quad (2)$$

for the phase shift detection. Here $|\alpha\rangle$ is a coherent state with the amplitude α and $K = 2(1 + e^{-2|\alpha|^2})$ is the corresponding normalization constant. Throughout, “the SC state” refers to the state defined in Eq. (2).

In Ref. [33], we considered using Fock states and SC states for this task while accounting for the finite quantum efficiency of photodetection. This inefficiency is equivalent to optical loss and can significantly degrade the observed non-Gaussian properties of the quantum states.

In the phase-space description, optical loss acts as Gaussian smoothing of the Wigner function [34]. Building on this picture, in Ref. [35] it was proposed to use anti-squeezing to protect the non-Gaussian nature of SC states; there the minimum value of the Wigner function served as the non-Gaussianity measure, and the predicted effect was later verified experimentally [36]. Related ideas were explored in Ref. [37], which instead quantified non-Gaussianity via the Wigner-negativity volume.

In this work, we continue the research of Refs. [32, 33]. We explore the use of antisqueezing-enhanced SC states to improve the robustness of our interferometric scheme to the optical losses. We take into account optical losses that occur both before the interferometer (in particular, the quantum state preparation inefficiency) and after it (in particular, the photodetection inefficiency). We perform numerical optimization of the antisqueezing degree for optimistic but experimentally achievable values of the Schrödinger cat amplitude and the

* valentine.gorshenin@yandex.ru

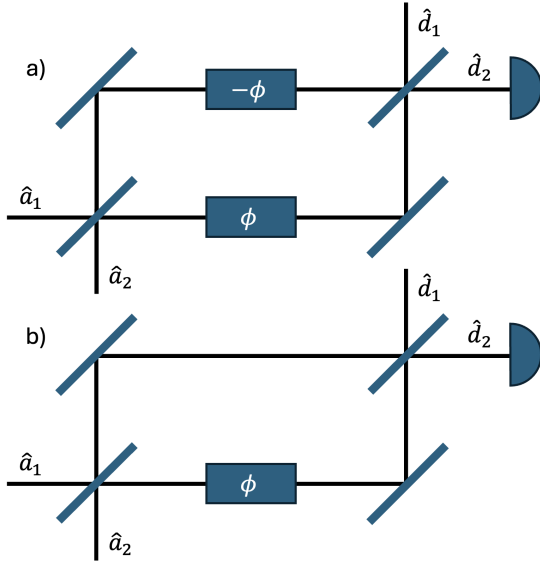


FIG. 1. Two equivalent implementations of the non-Gaussian interferometer: asymmetric (top) and antisymmetric (bottom) the Mach-Zehnder interferometer. \hat{a}_1 and \hat{d}_1 – bright input and output ports, \hat{a}_2 and \hat{d}_2 – dark input and output ports.

optical losses. We identify the ranges within which resulting sensitivity overcomes the one provided by the Gaussian squeezed states.

The paper is organized as follows. In Sec. II introduces the interferometric schemes considered in this paper. In Sec. III we analyze how the Wigner function of the probe light is affected the optical losses. In Sec. IV we calculate the photon-number statistics of the output optical state with account for the optical losses. In Sec. V we discuss the data processing procedure. In Sec. VI, we calculate the detection errors for a realistic implementation of our scheme. Finally, in Sec. VII we resume the results of the paper.

II. OPTICAL SCHEME

Following Ref. [32] we consider two standard configurations of the two-arm Mach-Zehnder interferometer (Fig. 1). In the asymmetric configuration, strongly unbalanced beam splitters are employed and the signal phase shift ϕ is imparted to a single arm. In the antisymmetric configuration, equal-magnitude phase shifts of opposite sign, $\pm\phi$, are applied to the two arms.

In both configurations, a classical coherent field enters through the bright input port, and a quantum state is injected through the dark input port. The interferometer is operated such that, when $\phi = 0$, the output states coincide with the input states at both the dark and bright ports.

In the regime of a small phase shift $\phi \ll \hbar/\langle \hat{n} \rangle$ (where $\langle \hat{n} \rangle$ – average energy passing through phase shift object) and weak quantum fluctuations, the bright output port field is insensitive to ϕ , while the state emerging from the dark port undergoes

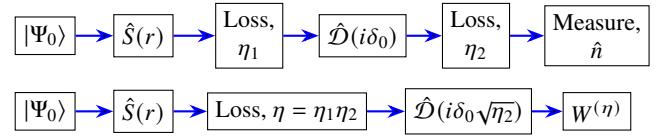


FIG. 2. (Top) Diagram of the lossy interferometer; (Bottom) Diagram of the equivalent simplified optical scheme

an effective displacement described by the operator:

$$\hat{D}(i\delta_0) = e^{i\delta_0(\hat{a}+\hat{a}^\dagger)}, \quad (3)$$

where \hat{a} denotes the annihilation operator and δ_0 is a dimensionless displacement parameter that scales with the bright-port coherent amplitude \sqrt{N} acting on the phase:

$$\delta_0 = \sqrt{N}\phi, \quad (4)$$

Here N is the mean photon number impinging on the phase-shifting element(s).

A schematic diagram of the interferometric scheme considered here is shown in Fig. 2 (top). We start with the SC state in Eq. (2). We then apply an anti-squeezing operation and inject the resulting state into the interferometer. The output state is measured using a photon-number-resolving (PNR) detector.

We account for optical loss by introducing two “loss” blocks in the diagram, placed before and after the interferometer and characterized by quantum efficiencies η_1 and η_2 , respectively. The first block accounts for losses introduced by the anti-squeezer as well as coupling (input) losses of the interferometer. The second block accounts for the interferometer output losses and the finite quantum efficiency of the photodetector. We model optical loss using the standard effective beam-splitter model [34].

It is shown in App. A that this optical scheme is equivalent to the simpler one with the single source of losses located before the interferometer, see Fig. 2 (bottom), and with the following effective parameters:

$$\text{effective loss factor: } \eta = \eta_1\eta_2, \quad (5a)$$

$$\text{effective signal: } \delta = \delta_0\sqrt{\eta_2}. \quad (5b)$$

In the Sec. III and Sec. IV we will use this effective model.

III. OPTICAL LOSSES

The Wigner function of a lossy anti-squeezed SC state has been derived in Ref. [38]; nevertheless, we present the main result here for completeness and to set the stage for the subsequent discussion. The wave function of the anti-squeezed and subsequently displaced Schrödinger-cat state, prior to optical loss, has the form

$$|\psi_{\text{sq, cat}}\rangle = \frac{1}{\sqrt{2(1 + \exp(-2|\alpha|^2))}} \hat{S}(r)(|\alpha\rangle + |-\alpha\rangle) \quad (6)$$

where the squeeze operator $\hat{S}(r)$ is defined as follows:

$$\hat{S}(r) = \exp\left(\frac{r}{2}(\hat{a}^2 - \hat{a}^{\dagger 2})\right) \quad (7)$$

Throughout, we use the convention that logarithmic squeeze parameter $r > 0$ corresponds to anti-squeezing and $r < 0$ to squeezing.

Wigner function after passing equivalent optical scheme presented on bottom panel of Fig. 1 (shown in the App. B) is follows:

$$W^{(\eta)}(x, p) = F(W_{\text{int}} + W_+ + W_-) \quad (8)$$

where the interference part W_{int} and the bell parts W_{\pm} of Wigner function are equal to

$$W_{\text{int}} = 2 \exp\left(-C - B(p - \delta)^2 - Ax^2\right) \cos\left(D(p - \delta)\right) \quad (9)$$

$$W_{\pm} = \exp\left(-A(x \pm \xi)^2 - B(p - \delta)^2\right), \quad (10)$$

where nonnegative coefficients A, B, C, D and F are defined as follows:

$$A = 2 \frac{s^2}{s^2(1 - \eta) + \eta}, \quad B = 2 \frac{1}{1 + (s^2 - 1)\eta}, \quad (11)$$

$$C = 2 \frac{\alpha^2(1 - \eta)}{1 + \eta(s^2 - 1)}, \quad D = \frac{4s\alpha\sqrt{\eta}}{1 + \eta(s^2 - 1)}, \quad (12)$$

$$F = \frac{s}{\pi(1 + e^{-2\alpha^2})} \sqrt{\frac{1}{(\eta(s^2 - 1) + 1)(s^2(1 - \eta) + \eta)}} \quad (13)$$

where $s \equiv e^r$. In the lossless and unsqueezed limit ($\eta = 1$, $s = 1$), they simplify to

$$A = B = 2, \quad C = 0, \quad D = 4\alpha, \quad F = \frac{1}{\pi(1 + e^{-2\alpha^2})} \quad (14)$$

which reproduces the Wigner function of the SC state in the absence of squeezing and loss (see Eq. (B1)).

A standard quantitative witness of nonclassicality is the Wigner negativity—the integrated “volume” of the negative region of the Wigner function. This negativity captures genuinely quantum aspects of the state that can sharpen distinguishability and, in favorable regimes, drive the overlap toward (near-)orthogonality. In this section, we develop an approximate approach for estimating the Wigner-negativity volume of large Schrödinger-cat states in the regime of large cat amplitude and pronounced antisqueezing.

To quantify the nonclassicality of the lossy SC state, we use the volume of the negative part of its Wigner function (Wigner negativity) V_{neg} defined by:

$$V_{\text{neg}} \equiv \frac{1}{2} \int_{-\infty}^{\infty} dx \int_{-\infty}^{\infty} dp \left(|W^{(\eta)}(x, p)| - W^{(\eta)}(x, p) \right) \quad (15)$$

This negativity captures genuinely quantum aspects of the state that can sharpen distinguishability and, in favorable regimes, drive the overlap toward (near-)orthogonality. In

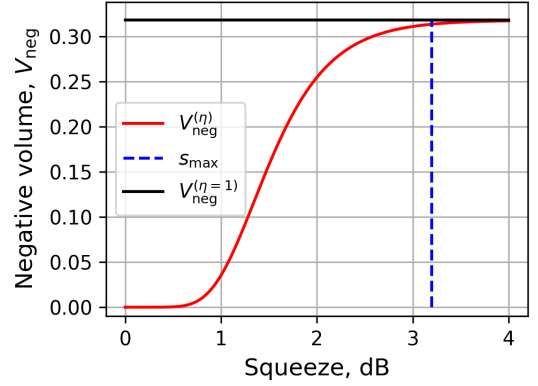


FIG. 3. Wigner negativity volume of V_{neg} the an anti-squeezed SC state versus the anti-squeezing level (in dB). Red solid curve: $\eta = 0.9$; black solid line: $\eta = 1$. In bothcases, $\alpha = 10$. The blue vertical dashed line marks the validity threshold of the approximation s_{max} , see Eq. (C5).

App. C, we develop an approximate approach for estimating the Wigner negativity volume of bright Schrödinger-cat states in the regime of large cat amplitude and performed antisqueezing.

$$V_{\text{neg}} = \frac{e^{-\frac{2\alpha^2(1-\eta)}{\eta(s^2-1)+1}}}{\pi(e^{-2\alpha^2} + 1)} \vartheta_3\left(\frac{\pi}{2}, e^{-\frac{2s^2\alpha^2\eta}{\eta(s^2-1)+1}}\right) \quad (16)$$

Fig. 3 plots the Wigner-negativity volume after loss versus the anti-squeezing factor s , for representative values of the SC state amplitude α and the loss parameter η . Notably, already at ~ 3 dB of anti-squeezing the Wigner negativity remains sizable, indicating that anti-squeezing can substantially mitigate loss-induced degradation.

IV. PHOTON-NUMBER STATISTICS OF OUTPUT STATE AFTER OPTICAL LOSSES

To incorporate the effect of optical loss in the output state into the phase-shift detection procedure, we need to calculate the photon-number probabilities p_n of the resulting state. We denote the corresponding density operator by $\hat{\rho}$. These probabilities can be obtained conveniently from a standard property of the Wigner function [4]:

$$p_n \equiv \text{Tr}(|n\rangle\langle n|\hat{\rho}) = 2\pi \int dx \int dp W_{\rho}(x, p) W_n(x, p), \quad (17)$$

where $W_n(x, p)$ is the Wigner function of the Fock state. The photon statistics of resulted state is follows (see for details App.

D):

$$\begin{aligned}
p_n = 4\pi \sum_{k=0}^{k=n} \sum_{m=0}^{m=k} \frac{n!}{k!(n-k)!} \frac{\sqrt{\pi} F 2^{2k+1} (-1)^{k+n}}{(A+2)^{m+\frac{1}{2}} (B+2)^{k-m+\frac{1}{2}}} \\
\exp\left(-\frac{2A\xi^2}{A+2} - \frac{D^2}{4B+8} - \frac{2B\delta^2}{B+2} - C\right) \cdot \\
\cdot \left(\sqrt{\pi} e^{\frac{D^2}{4B+8} + C} L_m^{-\frac{1}{2}}\left(-\frac{A^2\xi^2}{A+2}\right) L_{k-m}^{-\frac{1}{2}}\left(-\frac{B^2\delta^2}{B+2}\right) + \right. \\
\left. + e^{\frac{2A\xi^2}{A+2}} \frac{\Gamma\left(m+\frac{1}{2}\right)}{m!} \operatorname{Re}\left(e^{\frac{2iD\delta}{B+2}} L_{k-m}^{-\frac{1}{2}}\left(\frac{(D+2iB\delta)^2}{4(B+2)}\right)\right)\right) \quad (18)
\end{aligned}$$

Numerical evaluation of the ratio $\Gamma(m+1/2)/m!$ slightly complicates the computation of the photon-number statistics. Using Stirling's approximation, we derive a simpler expression that is accurate and numerically stable; see the end of App. D.

The alternative approach to calculation of the photon number statistics is the use of the binomial conditional photon number probabilities introduced by the loss sources. However, this method does not readily accommodate sequences of the form loss \rightarrow linear operation (displacement, squeezing and phase shift) \rightarrow loss. Therefore, to validate our approximate approach, in App. E we compare the both methods in a simpler setting: a displaced and squeezed SC state followed by a single source of losses and show that their results coincide with very good precision.

V. DATA PROCESSING ALGORITHM

In a single-shot setting, the decision must be made from a single observed photon count n , rather than from an estimated distribution. In Ref. [32], a simple decision strategy for determining the presence or absence of a phase shift based on photon-number parity was used. However, it becomes suboptimal in the presence of optical loss. In Ref. [33], we proposed using the maximum-likelihood method. We use this method here as well.

We assign each measured photon number to one of the two hypotheses: absence or presence of a phase shift [17, 39]. For binary discrimination between the nondisplaced state $\hat{\rho}_0$ and the displaced state $\hat{\rho}_\delta$, we consider their photon-number distributions:

$$p_n^{(0)} \equiv \operatorname{Tr}(\hat{\rho}_0 |n\rangle\langle n|) \quad p_n^{(\delta)} \equiv \operatorname{Tr}(\hat{\rho}_\delta |n\rangle\langle n|) \quad (19)$$

We therefore partition the nonnegative integers into two decision regions, N_0 and N_δ associated with the hypotheses "phase shift absence" and "phase shift present", respectively. For a single-shot defined decision rule, these regions must form a complete partition of the Fock-state index set. We assign n according to the maximum-likelihood (ML) decision rule:

$$n \in N_0 \iff p_n^{(0)} > p_n^{(\delta)}, \quad n \in N_\delta \iff p_n^{(0)} < p_n^{(\delta)} \quad (20)$$

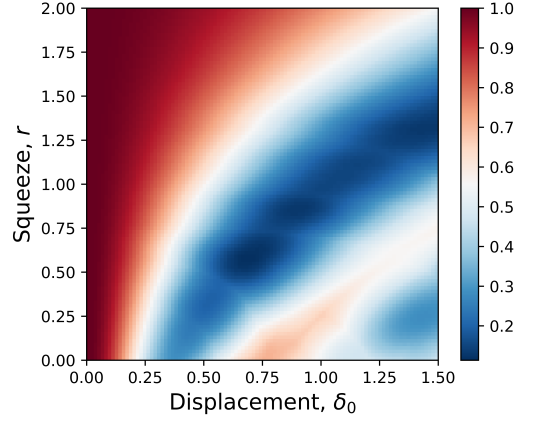


FIG. 4. Total error probability p_{tot} as a function of the displacement δ_0 and antisqueeze factor r for $\alpha = 2.0$ and $\eta = 0.975$.

We define the false-positive and false-negative error probabilities, p_{fp} and p_{fn} , as follows:

$$p_{\text{fp}} = \sum_{n \in N_\delta} p_n^{(0)}, \quad p_{\text{fn}} = \sum_{n \in N_0} p_n^{(\delta)} \quad (21)$$

The corresponding total error is defined as:

$$p_{\text{tot}} \equiv p_{\text{fn}} + p_{\text{fp}}. \quad (22)$$

VI. ESTIMATES OF THE ERROR PROBABILITIES

We proceed to estimate the false-positive and false-negative error probabilities, adopting reasonably optimistic parameter values for our scheme. Because the method introduced in Sec. II becomes computationally intractable for photon number higher than 23 in the following numerical calculation, we instead employ a binomial method for loss consideration. This restriction precludes the inclusion of SC states with large amplitudes. We consider displacement with argument $i\delta_0$ and losses after it η on anti-squeezed SC state.

Concerning the quantum efficiency η , over the past several decades, considerable progress has been made in developing photon-number-resolving (PNR) detectors. The best values of η are currently obtained with cryogenic photon-counting technologies, most notably superconducting nanowire detectors and transition-edge sensors (TESs). The former ones can reach efficiencies as high as 95% while resolving on the order of 20 photons [40]. TES-based PNR detectors can achieve efficiencies up to 98% and resolve up to ~ 100 photons [41–43].

Regarding the input quantum state preparation, experimentally demonstrated SC states preparation protocols typically achieve amplitudes $\alpha \leq 1.5$ [36, 44–46]. Looking ahead, PNR-detectors based schemes for generating brighter SC states have been proposed, with target amplitudes on the order of $\alpha \approx 4-5$ [47, 48].

The values of squeezing, experimentally attainable in transient crystals, is typically in the range 5–10 dB, which corresponds to r in the range $0.57 \leq r \leq 1.15$ [36, 49–51].

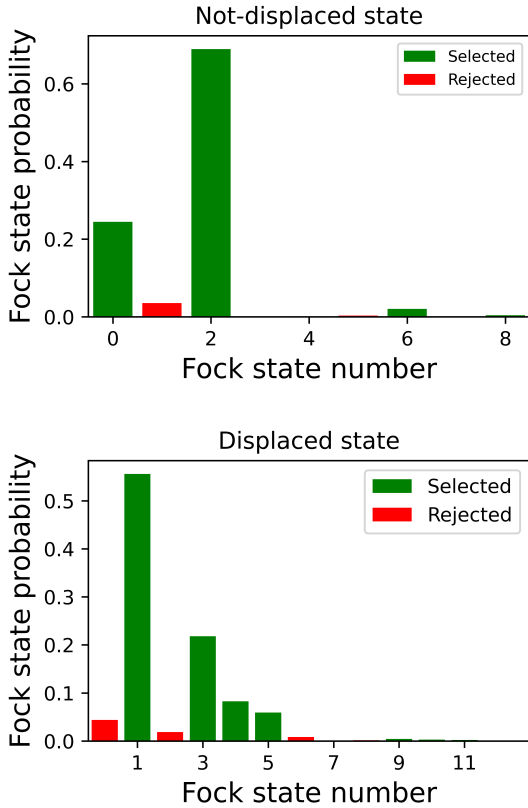


FIG. 5. Photon-number distributions of the optimized anti-squeezed SC state for the case of $\alpha = 2.0$ and $\eta = 0.975$, $r = 0.56$ (5 dB). Top: no signal, $\delta_0 = 0$, bottom: with signal, $\delta_0 = 0.68$. The red bars constitute the detection error.

In Fig. 4, the detection error p_{tot} is plotted as a function of δ_0 and r for the particular case of $\alpha = 2$ and $\eta = 0.975$. This plots shows several minima of the total detection error p_{tot} . The best value (for these specific parameters) is close to $p_{\text{tot}} \approx 0.1$ and can be reached using moderate anti-squeezing of ≈ 5 dB at $\delta_0 \approx 0.7$.

The corresponding photon-number distributions of the SC state (after losses) for the cases of the absence and the presence of the signal are plotted in Fig. 5.

A more general view on the sensitivity is provided by Fig. 6, where p_{tot} is plotted as a function of the quantum efficiency η and the SC amplitude α . For each pair of these arguments, the global minimum of p_{tot} in (δ_0, r) is calculated and presented in the plot.

In Fig. 7, the corresponding optimized factor r is plotted as a function of η and α , showing that the required anti-squeezing tends to decrease with the increase of η and, for the considered here values of η and α , never exceeds ≈ 14 dB.

In order to demonstrate the advantage provided by the non-Gaussian SC state, we compare the achievable sensitivity with the one provided by the Gaussian squeezed states with the equivalent value of the squeeze factor, equal by the absolute value to the factor r used in the previous estimates, assuming the same quantum efficiency η . It is shown in App. F that the

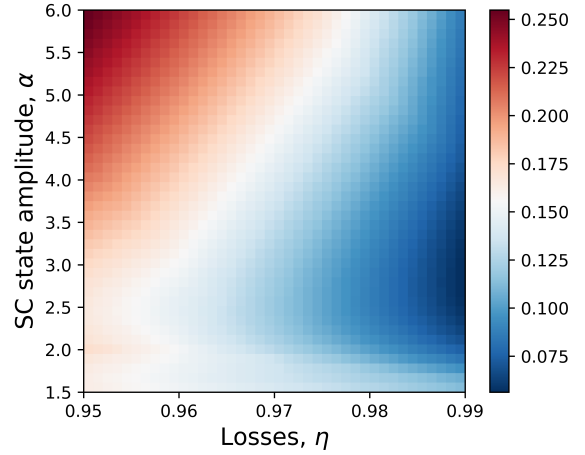


FIG. 6. Total error probability p_{tot} as a function of the SC state amplitude α and the quantum efficiency η . For each (α, η) , the displacement δ_0 and antisqueezing parameter r are optimized.

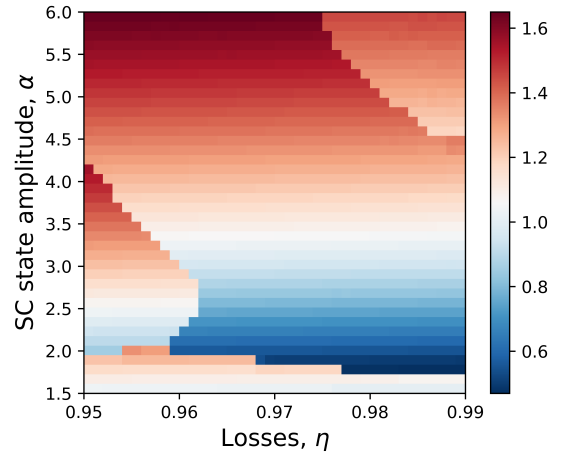


FIG. 7. The optimal antisqueezing r as a function of the SC state amplitude α and the quantum efficiency η .

corresponding error probability for detection of a given phase shift is equal to

$$p_{\text{sq}} = \text{erfc} \left(\delta_0 \sqrt{\frac{\eta}{2\eta(s^2 - 1) + 2}} \right). \quad (23)$$

In Fig. 8, the corresponding ratio $p_{\text{tot}}/p_{\text{sq}}$ is plotted as a function of α and η . For each pair (α, η) , the optimal values of δ_0 , r are used, similar to how it done in Fig. 6. It can be seen from this plot, that in the case of small losses, the SC state could provide several times better sensitivity.

The code which was used for obtaining these results is provided in the GIT repository [52].

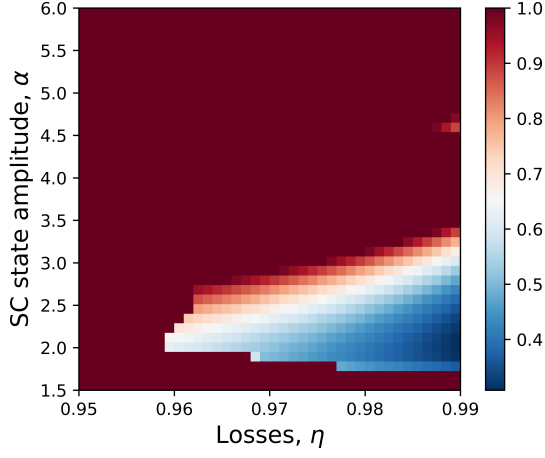


FIG. 8. The ratio of the detection errors for the SC state and Gaussian squeezed state $p_{\text{tot}}/p_{\text{sq}}$ as a function of α and η . For each (α, η) , the displacement δ_0 and antisqueezing parameter r are optimized. To emphasize the regime in which the SC state beats the squeezed vacuum one, the values of $p_{\text{tot}}/p_{\text{sq}} > 1$ are displayed as 1.

VII. CONCLUSION

We showed here that using anti-squeezed Schrödinger cat probe states in the non-Gaussian interferometric scheme proposed in Refs. [32, 33], it is possible to make this scheme significantly more tolerant to optical losses.

In our analysis, we assumed the use of the modern photon-number-resolving detectors and the maximum likelihood decision rule. We performed numerical optimization of the anti-squeezing factor assuming optimistic but experimentally achievable values of the Schrödinger cat amplitude α and the quantum efficiency of the setup η and identified the area in these parameters space within which the resulting sensitivity overcomes the one provided by the Gaussian squeezed states. Note that this area corresponds to demanding but feasible values of $\eta \gtrsim 0.96$ and SC-state amplitudes $1.5 \leq \alpha \leq 3$.

ACKNOWLEDGMENTS

This work was supported by the Foundation for the Advancement of Theoretical Physics and Mathematics (“BASIS” Grant 23-1-1-39-1). The authors would like to express his deep gratitude to F. Ya. Khalili for his invaluable contributions to the discussions.

Appendix A: Two sequential photon losses

Consider the the following sequence:

$$\hat{U} = \hat{\mathcal{L}}_2 \hat{\mathcal{D}}(i\delta_0) \hat{\mathcal{L}}_1, \quad (\text{A1})$$

where $\mathcal{D}(i\delta_0)$ is the displacement operator (3), $\hat{\mathcal{L}}_i$, with $i = 1, 2$, are the evolution operators describing the optical losses

as follows:

$$\hat{\mathcal{L}}_i^\dagger \hat{a} \hat{\mathcal{L}}_i = \sqrt{\eta_i} \hat{a} + \sqrt{1 - \eta_i} \hat{z}_i, \quad (\text{A2a})$$

$$\hat{\mathcal{L}}_i^\dagger \hat{z}_i \hat{\mathcal{L}}_i = \sqrt{\eta_i} \hat{z}_i - \sqrt{1 - \eta_i} \hat{a}, \quad (\text{A2b})$$

and $\hat{z}_{1,2}$ are the annihilation operators of the two vacuum modes. Using the unitarity of the operator $\hat{\mathcal{L}}_2$ and Eq. (A2a), we obtain that

$$\hat{U} = \hat{\mathcal{L}}_2 \hat{\mathcal{D}}(i\delta_0) \hat{\mathcal{L}}_2^\dagger \hat{\mathcal{L}}_2 \hat{\mathcal{L}}_1 = \hat{\mathcal{D}}(i\delta_0 \sqrt{\eta_2}) \hat{\mathcal{D}}_{\text{loss}} \hat{\mathcal{L}}, \quad (\text{A3})$$

where

$$\hat{\mathcal{D}}_{\text{loss}} = e^{i\delta_0 \sqrt{1 - \eta_1} (\hat{z}_1 - \hat{z}_1^\dagger)}, \quad \hat{\mathcal{L}} = \hat{\mathcal{L}}_2 \hat{\mathcal{L}}_1. \quad (\text{A4})$$

Note that

$$\hat{\mathcal{L}}^\dagger \hat{a} \hat{\mathcal{L}} = \sqrt{\eta_2} (\sqrt{\eta_1} \hat{a} + \sqrt{1 - \eta_1} \hat{z}_1) + \sqrt{1 - \eta_2} \hat{z}_2 = \sqrt{\eta} \hat{a} + \sqrt{1 - \eta} \hat{z}, \quad (\text{A5})$$

where

$$\eta = \eta_1 \eta_2, \quad \hat{z} = \frac{\sqrt{(1 - \eta_1) \eta_2} + \sqrt{1 - \eta_2}}{\sqrt{1 - \eta_1 \eta_2}} \quad (\text{A6})$$

are the unified quantum efficiency and the corresponding effective noise, compare with Eq. (A2a). Note also that $\hat{\mathcal{D}}_{\text{loss}}$ is a unitary operator acting only in the first losses mode subspace and therefore vanishes when calculating the output state of the signal mode:

$$\begin{aligned} \hat{\rho}_{\text{signal out}} &= \text{Tr}_{\text{loss}}(\hat{U} \hat{\rho}_{\text{signal in}} \otimes \hat{\rho}_{\text{loss}} \hat{U}^\dagger) = \\ &= \text{Tr}_{\text{loss}}(\hat{\mathcal{D}}(i\delta_0 \sqrt{\eta_2}) \hat{\mathcal{L}} \hat{\rho}_{\text{signal in}} \otimes \hat{\rho}_{\text{loss}} \hat{\mathcal{L}}^\dagger \hat{\mathcal{D}}^\dagger(i\delta_0 \sqrt{\eta_2})). \end{aligned} \quad (\text{A7})$$

where $\hat{\rho}_{\text{signal in}}$ and $\hat{\rho}_{\text{loss}}$ are the initial states of the signal and the loss modes and Tr_{loss} means tracing out the loss modes.

This result corresponds to the action of the unified losses with the quantum efficiency (A6) followed by the lossless evolution of the signal mode, with the displacement factor scaled by $\sqrt{\eta_2}$.

Appendix B: Derivation of Wigner function after passing equivalent optical scheme

The corresponding Wigner function for the state $|\psi_{\text{sq, cat}}\rangle$ (see Eq. (6)) is given by

$$\begin{aligned} W(x, p) &= \frac{2}{\pi K} \left\{ \exp\left(-2(xs - \alpha)^2 - 2(p/s)^2\right) + \right. \\ &\quad \left. + \exp\left(-2(xs + \alpha)^2 - 2(p/s)^2\right) + \right. \\ &\quad \left. + 2 \exp\left(-2(xs)^2 - 2(p/s)^2\right) \cos\left(4\alpha p/s\right) \right\} \end{aligned} \quad (\text{B1})$$

where $s \equiv e^r$.

Taking into account the input losses (see Ref. [34]), we obtain the following Wigner function of the effective input state of the interferometer:

$$W^{(\eta)}(x, p) = \iint W(u, v) B(x - \sqrt{\eta}u, p - \sqrt{\eta}v, \eta) dudv, \quad (\text{B2})$$

where

$$B(x, p, \eta) = \frac{2}{\pi(1-\eta)} \exp\left(-\frac{2(x^2 + p^2)}{1-\eta}\right) \quad (\text{B3})$$

is the a ‘‘Gaussian blurring filter’’.

This Wigner function can be presented as follows:

$$W^{(\eta)} = F(W_{\text{int}} + W_+ + W_-), \quad (\text{B4})$$

where we have introduced the ‘‘bell’’ terms $W_{\pm}(x, p)$, corresponding to the two coherent-state components, and the interference term $W_{\text{int}}(x, p)$ of the Wigner function:

$$W_{\pm} = \exp\left(-A(x \pm \xi)^2 - Bp^2\right) \quad (\text{B5})$$

$$W_{\text{int}} = 2 \exp\left(-C - Bp^2 - Ax^2\right) \cos(Dp) \quad (\text{B6})$$

where we have introduced the effective SC-state amplitude after loss, $\xi = \frac{\alpha\sqrt{\eta}}{s}$. The nonnegative coefficients A, B, C, D and F are presented in Eq. (11).

After applying the displacement operator with the displacement parameter $\delta = \delta_0\sqrt{\eta/2}$, we obtain the same functional form of the Wigner function (see Eq. (B4)), but with slightly modified bell and interference terms (see Eq. (9) and Eq. (10))

Appendix C: Derivation of negative volume of anti-squeezed SC state after losses (Eq. (16))

To obtain an analytical estimate of the Wigner negativity, we make the following approximations. first, we keep only the interference contribution, Eq. (9), and drop the two Gaussian bells terms in Eq. (10). We discuss the regime of validity of this simplification in the end of this section. With this approximation, the negativity volume becomes

$$V_{\text{neg}} = \frac{1}{2} \int_{-\infty}^{\infty} dx \int_{-\infty}^{\infty} dp (|W_{\text{int}}(x, p)| - W_{\text{int}}(x, p)) \quad (\text{C1})$$

Second, in the case of bright enough SC state, the interference fringes in the Wigner function [Eq. (9)] are much finer than the width of the Gaussian envelope associated with the two lobes. Because $W_{\text{int}} \sim \exp(-D(y - \delta)) \cos(D(p - \delta))$ it oscillates rapidly across momentum axis, generating alternating positive and negative fringes within slightly changing envelope during one cosine period:

$$W_{\text{int}} \sim \cos(D(p - \delta)) \exp(-D(p - \delta)^2), \quad (\text{C2})$$

Accordingly, we restrict the integration domain to the negative-fringe regions where $W_{\text{int}}(x, p) < 0$, i.e., where $\cos(D(p - \delta)) < 0$. In the case of bright enough SC state, the cosine fringes are fast compared with the variation scale of the Gaussian envelope, so the integral over phase space can be evaluated by decomposing it into a sum over individual negative half-periods and treating the Gaussian envelope as

approximately constant within each half-period. Under this slowly varying envelope approximation, the integral becomes

$$V_{\text{neg}} = 2 \exp(-C) \int \exp(-Ax^2) dx \sum_{k=-\infty}^{k=\infty} \exp(-B(p_k - \delta)^2) \cdot \int_{p_k - \pi/(2D)}^{p_k + \pi/(2D)} \cos(D(p - \delta)) dy = 4\vartheta_3(\exp(-((4B\pi^2)/D^2))) \quad (\text{C3})$$

where $p_k = \delta + 2\pi k/D$, ($k \in \mathbb{Z}$), denote the positions of the cosine minima, and $\vartheta_3(x)$ is the Jacobi theta-function

Our simplified treatment rests on two assumptions. First, the interference contribution W_{int} , which carries the Wigner negativity, is well separated in phase space from the positive Gaussian bell terms W_{\pm} . This negligible-overlap condition can be estimated using a standard three-sigma criterion where σ – is standard deviation of two terms of Wigner function along x axis:

$$\sigma_{\text{bell},x} = \frac{1}{\sqrt{2A}}; \sigma_{\text{int},x} = \frac{1}{\sqrt{2A}} \quad (\text{C4})$$

Substituting the parameters given in Eq. (11) and simplify yields the condition

$$\frac{3\alpha\sqrt{\eta}\sqrt{(\eta(s^2 - 1) + s^2)}}{s^2} < 1 \quad (\text{C5})$$

The corresponding anti-squeezing threshold $s = s_{\text{max}}$, defined by saturating the inequality, is also marked in Fig. 3.

Our second approximation treats the slowly varying Gaussian envelope as approximately constant on the scale of a single interference fringe. We assess the regime of validity by comparing the exact expression in Eq. (9) with the corresponding approximation at $x = 0$:

$$f_{\text{fine}}(p) \equiv 2e^{-C} e^{-B(p-\delta)^2} \cos(D(p-\delta)) \quad (\text{C6})$$

$$f_{\text{approx}}(p) \equiv 2e^{-C} \sum_{k=-\infty}^{k=\infty} e^{-B(2\pi k/D)^2} \cos(D(p-\delta)) \cdot \theta(p-\delta - 2\pi k/D) \theta(-p+\delta + 2\pi(k+1)/D) \quad (\text{C7})$$

where $\theta(x)$ is Heaviside theta-function.

A convenient measure of the agreement is the inner product between $f_{\text{fine}}(p)$ and $f_{\text{approx}}(p)$, evaluated over the real line:

$$I = \frac{\langle f_{\text{fine}}, f_{\text{approx}} \rangle}{\sqrt{\langle f_{\text{fine}}, f_{\text{fine}} \rangle \langle f_{\text{approx}}, f_{\text{approx}} \rangle}} \quad (\text{C8})$$

where denominator corresponds normalization constant. Inner product defined as follows:

$$\langle f, g \rangle \equiv \int_{-\infty}^{\infty} f_{\text{fine}}(p) f_{\text{approx}}(p) dp \quad (\text{C9})$$

We report high enough inner product value $\langle f_{\text{fine}}(p), f_{\text{approx}}(p) \rangle$. For example for $\eta = 0.9$ the

overlap is higher than 99.9% for SC amplitudes $\alpha > 6$ and anti-squeeze in range from 4 to 10 dB and losses. The lowest overlap value is equal to 99.8% for small SC state amplitudes $\alpha = 4$ which tell of approximation correctness. This indicates that $f_{\text{approx}}(p)$ provides an accurate representation of $f_{\text{fine}}(p)$ and justifying the approximation used to estimate the Wigner-negativity volume.

Appendix D: Derivation of Eq. (18)

Wigner function $W_n(x, p)$ is the n -photon Fock state equal to

$$W_n(x, p) = \frac{2}{\pi} (-1)^n e^{-2(x^2+p^2)} L_n(4(x^2+p^2)) \quad (\text{D1})$$

and

$$L_n(z) = \sum_{k=0}^{k=n} \frac{(-1)^k}{k!} \frac{n!}{(n-k)!k!} z^k \quad (\text{D2})$$

is the Laguerre polynomial.

Using the binomial expansion for powers of $z = 4(x^2 + y^2)$, the Wigner function of the Fock state Laguerre polynomial can be written as

$$L_n(4(x^2+p^2)) = \sum_{k=0}^{k=n} \sum_{m=0}^{m=k} \frac{4^k (-1)^k n!}{k!(n-k)!} \frac{1}{(k-m)!m!} x^{2m} p^{2(k-m)} \quad (\text{D3})$$

To calculate the photon-number probabilities according Eq. (17), we need to evaluate integrals of the form

$$I_{\text{int}}^{(k,m)} = \int_{\mathbb{R}} \int_{\mathbb{R}} \cos(D(p-\delta)) \cdot \exp(-Ax^2 - B(p-\delta)^2) e^{-2(x^2+p^2)} x^{2m} p^{2(k-m)} dx dp \quad (\text{D4})$$

$$I_{\text{bell},\pm}^{(k,m)} = \int_{\mathbb{R}} \int_{\mathbb{R}} \exp(-C - A(x \pm \xi)^2 - B(p-\delta)^2) \cdot e^{-2(x^2+p^2)} x^{2m} p^{2(k-m)} dx dp. \quad (\text{D5})$$

As a result, we obtain:

$$p_n = 4\pi F \sum_{k=0}^{k=n} \sum_{m=0}^{m=k} \frac{4^k (-1)^k n!}{k!(n-k)!} \frac{I_{\text{int}}^{(k,m)} + I_{\text{bell},+}^{(k,m)} + I_{\text{bell},-}^{(k,m)}}{(k-m)!m!}, \quad (\text{D6})$$

Using Wolfram Mathematica integrals (D4) and (D5) could be calculated in the following form:

$$I_{\text{bell},\pm}^{(k,m)} = \frac{\Gamma\left(m + \frac{1}{2}\right) \Gamma\left(k - m + \frac{1}{2}\right)}{(A+2)^{m+\frac{1}{2}} (B+2)^{k-m+\frac{1}{2}}} e^{-A\xi^2 - B\delta^2}. \quad (\text{D7})$$

$$\cdot {}_1F_1\left(m + \frac{1}{2}; \frac{1}{2}; \frac{A^2\xi^2}{A+2}\right) {}_1F_1\left(k - m + \frac{1}{2}; \frac{1}{2}; \frac{B^2\delta^2}{B+2}\right) \quad (\text{D8})$$

$$I_{\text{int}}^{(k,m)} = 2 \frac{\Gamma\left(m + \frac{1}{2}\right) \Gamma\left(k - m + \frac{1}{2}\right)}{(A+2)^{m+\frac{1}{2}} (B+2)^{k-m+\frac{1}{2}}} e^{-2B\delta^2 - C - B\delta^2}. \quad (\text{D9})$$

$$\cdot \text{Re}\left(e^{-iD\delta} {}_1F_1\left(k - m + \frac{1}{2}; \frac{1}{2}; \frac{(iD+2B\delta)^2}{4(B+2)}\right)\right) \quad (\text{D10})$$

Known properties could be used:

$$\Gamma\left(\frac{1}{2} + n\right) {}_1F_1\left(n + \frac{1}{2}; \frac{1}{2}; z\right) = \sqrt{\pi} e^z n! L_n^{-1/2}(-z) \quad (\text{D11})$$

After this Eqs. (D7), (D9) slightly simplifies:

$$I_{\text{bell},\pm}^{(k,m)} = \frac{\pi m!(k-m)! \exp\left(-\frac{2A\xi^2}{A+2} - \frac{2B\delta^2}{B+2}\right)}{(A+2)^{m+\frac{1}{2}} (B+2)^{k-m+\frac{1}{2}}} \cdot L_m^{-\frac{1}{2}}\left(-\frac{A^2\xi^2}{A+2}\right) L_{k-m}^{-\frac{1}{2}}\left(-\frac{B^2\delta^2}{B+2}\right) \quad (\text{D12})$$

$$I_{\text{int}}^{(k,m)} = \frac{2\sqrt{\pi} \Gamma\left(m + \frac{1}{2}\right) (k-m)!}{(B+2)^{k-m+\frac{1}{2}} (A+2)^{m+\frac{1}{2}}} \cdot \exp\left(-\frac{4(B+2)C + 8B\delta^2 + D^2}{4(B+2)}\right) \cdot \text{Re}\left(\exp\left(iD\delta - \frac{iBD\delta}{B+2}\right) L_{k-m}^{-\frac{1}{2}}\left(\frac{(D+2iB\delta)^2}{4(B+2)}\right)\right) \quad (\text{D13})$$

After substituting Eqs. (D12) and (D13) into Eq. (D6) and simplifying, we obtain Eq. (18).

This expression can be simplified using Stirling's approximation, which reduces numerical round-off errors and yields a more tractable form [53]:

$$n! = \sqrt{2\pi n} \left(\frac{n}{e}\right)^n \exp\left(\frac{1}{12n} + \frac{1}{288n^2}\right) \quad (\text{D14})$$

After this we obtain:

$$\frac{(2m)!}{(m!)^2} \approx \frac{2^{2m}}{\sqrt{\pi m}} S, \quad (\text{D15})$$

where was introduced:

$$S = \exp\left(-\frac{144n+7}{1152n^2}\right) \quad (\text{D16})$$

According this:

$$\frac{\Gamma\left(\frac{1}{2} + n\right)}{n!} = \frac{(2n)!}{4^n (n!)^2} \sqrt{\pi} = \frac{S}{\sqrt{n}} \quad (\text{D17})$$

After substituting into the equation (18) and reducing the terms, we obtain:

$$p_n = \sum_{k=0}^{k=n} \sum_{m=0}^{m=k} \frac{4\pi n!}{k!(n-k)!} \frac{\pi F 2^{2k+1} (-1)^{k+n}}{(A+2)^{m+\frac{1}{2}} (B+2)^{k-m+\frac{1}{2}}} \cdot \exp\left(-\frac{2A\xi^2}{A+2} - \frac{D^2}{4B+8} - \frac{2B\delta^2}{B+2} - C\right) \cdot \left(e^{\frac{D^2}{4B+8} + C} L_m^{-\frac{1}{2}}\left(-\frac{A^2\xi^2}{A+2}\right) L_{k-m}^{-\frac{1}{2}}\left(-\frac{B^2\delta^2}{B+2}\right) + e^{\frac{2A\xi^2}{A+2}} \frac{S}{\sqrt{m}} \text{Re}\left(e^{\frac{2iD\delta}{B+2}} L_{k-m}^{-\frac{1}{2}}\left(\frac{(D+2iB\delta)^2}{4(B+2)}\right)\right)\right) \quad (\text{D18})$$

We use this approximation in our numerical calculations when the parameter $m > 20$. We also note a practical limitation of the numerical procedure: the photon-number statistics can be computed reliably only up to a cutoff of $n \leq 23$. For larger cutoffs, the calculation becomes numerically unstable and the accumulated round-off error becomes significant.

Appendix E: Comparison of proposed in Sec. IV photon statistics calculation method and combinatorial method

An alternative way to incorporate optical loss is to introduce conditional photon-counting probabilities. Below we compare with this approach. Let the input (pre-loss) state be described by the density operator ρ_{in} in the Fock basis. In the absence of loss, the probability of detecting n photons is the diagonal element $p_n = (\rho_{\text{in}})_{n,n}$. Optical loss transforms the photon-number distribution according to

$$p_n^{(\eta)} = \sum_{m=n}^{\infty} P(n|m) p_m, \quad (\text{E1})$$

where

$$P(n|m) = \frac{m!}{n!(m-n)!} (1-\eta)^{m-n} \eta^n. \quad (\text{E2})$$

To assess the accuracy of the Wigner-function-based photon-statistics method (Eqs. (18) and (D18)), we define the probability difference

$$\Delta = \sum_n |p_{n,\text{analytical}} - p_{n,\text{combinatoric}}| \quad (\text{E3})$$

We report small value of error of proposed method of photon statistics calculation Δ (see Eq. (E3)). For example consider for SC state with amplitude $\alpha = 1.5$ and losses $\eta = 0.85$. For band of squeeze $0 \leq r \leq 1.2$ and displacement $0 \leq \delta_0 \leq 1.5$ the maxim error is achieves $\Delta = 0.002$ for squeeze near zero. For the rest areas average error $\Delta \leq 0.001$.

Appendix F: Derivation of Eq. (23)

For comparison of proposed protocol we will compare it with an equally squeezed vacuum state. For this consideration we consider that vacuum state pass into considering optical scheme (top panel) presented in Fig. 1 and equivalent to it (bottom panel). In result vacuum state is squeezed, enforced to optical losses and was displaced. For comparison we consider the homodyne measurement of momentum for detection of given phase shift. In that case we aim to obtain momentum probability representation of resultig state.

The Wigner function of the displaced squeezed vacuum state is as follows:

$$W_{\delta,\text{sq}}(x, p) = \frac{2e^{-2s^2x^2 - \frac{2(p-\delta_0)^2}{s^2}}}{\pi} \quad (\text{F1})$$

where $s = e^{-r}$ denotes squeeze parameter along the momentum quadrature, rather than anti-squeezing as in the SC-state analysis.

Similar to the similar Sec. III after ‘‘Gaussian blurring filter’’ Wigner function is as follows:

$$W_{\delta,\text{sq}}^{(\eta)}(x, p) = \frac{2s \exp\left(-\frac{2s^2x^2}{\eta - \eta s^2 + s^2} - \frac{2(p - \sqrt{\eta}\delta_0)^2}{\eta(s^2 - 1) + 1}\right)}{\pi \sqrt{(\eta - (\eta - 1)s^2)(\eta(s^2 - 1) + 1)}} \quad (\text{F2})$$

For procedure of detection we will consider homodyne measurement of momentum. It could be found easily from Wigner function as follows:

$$\omega(p) = \frac{\sqrt{2}e^{-\frac{2(y - \sqrt{\eta_2}\delta_0)^2}{\eta(s^2 - 1) + 1}}}{\sqrt{\pi\eta(s^2 - 1) + \pi}} \quad (\text{F3})$$

We aim to discriminate non-displaced and displaced SC states. According this reasonable to select point between two Gaussian peaks along momentum axis which is border p_{border} between displaced and non-displaced $\delta_0 = 0$ state:

$$p_{\text{border}} = \sqrt{\eta_2}\delta_0/2 \quad (\text{F4})$$

Assume that value δ_0 is positive. In the case of measuring momentum higher(lower) than y_0 we detect presense(absence) of phase shift. According this false positive $p_{\text{fp}}^{(\text{sq})}$ and false negative $p_{\text{fn}}^{(\text{sq})}$ errors could be introduced as follows:

$$p_{\text{fp}}^{(\text{sq})} = \int_{p=p_{\text{border}}}^{\infty} \omega(p) dp, \quad p_{\text{fn}}^{(\text{sq})} = \int_{-\infty}^{p=p_{\text{border}}} \omega(p) \Big|_{\delta_0=0} dp \quad (\text{F5})$$

After calculating of integrals we obtain and assuming $\eta_1 = 1$ and $\eta_2 = \eta$:

$$p_{\text{fp}}^{(\text{sq})} = p_{\text{fn}}^{(\text{sq})} = \frac{1}{2} \text{erfc}\left(\delta_0 \sqrt{\frac{\eta}{2\eta(s^2 - 1) + 2}}\right) \quad (\text{F6})$$

Total error for squeezed states $p_{\text{sq}} \equiv p_{\text{fp}}^{(\text{sq})} + p_{\text{fn}}^{(\text{sq})}$ is has form Eq. (23).

-
- [1] U. L. Andersen, O. Glöckl, T. Gehring, and G. Leuchs, Quantum interferometry with gaussian states, in [Quantum Information](#) (John Wiley & Sons, Ltd, 2019) Chap. 35, pp. 777–798, <https://onlinelibrary.wiley.com/doi/pdf/10.1002/9783527805785.ch35>
- [2] D. Salykina and F. Khalili, Sensitivity of quantum-enhanced interferometers, [Symmetry](#) **15**, 774 (2023).
- [3] C. M. Caves, Quantum-mechanical noise in an interferometer, [Phys. Rev. D](#) **23**, 1693 (1981).
- [4] W. Schleich, [Quantum Optics in Phase Space](#) (WILEY-VCH, Berlin, 2001) p. 695.

- [5] M. J. Holland and K. Burnett, Interferometric detection of optical phase shifts at the heisenberg limit, *Phys. Rev. Lett.* **71**, 1355 (1993).
- [6] H. Lee, P. Kok, and J. P. Dowling, A quantum rosetta stone for interferometry, *Journal of Modern Optics* **49**, 2325 (2002), <https://doi.org/10.1080/0950034021000011536>.
- [7] R. A. Campos, C. C. Gerry, and A. Benmoussa, Optical interferometry at the heisenberg limit with twin fock states and parity measurements, *Phys. Rev. A* **68**, 023810 (2003).
- [8] D. W. Berry, B. L. Higgins, S. D. Bartlett, M. W. Mitchell, G. J. Pryde, and H. M. Wiseman, How to perform the most accurate possible phase measurements, *Phys. Rev. A* **80**, 052114 (2009).
- [9] L. Pezzé and A. Smerzi, Ultrasensitive two-mode interferometry with single-mode number squeezing, *Phys. Rev. Lett.* **110**, 163604 (2013).
- [10] M. Perarnau-Llobet, A. González-Tudela, and J. I. Cirac, Multi-mode Fock states with large photon number: effective descriptions and applications in quantum metrology, *Quantum Science and Technology* **5**, 025003 (2020), [arXiv:1910.03323 \[quant-ph\]](https://arxiv.org/abs/1910.03323).
- [11] G. Shukla, K. M. Mishra, A. K. Pandey, T. Kumar, H. Pandey, and D. K. Mishra, Improvement in phase-sensitivity of a mach-zehnder interferometer with the superposition of schrödinger's cat-like state with vacuum state as an input under parity measurement, *Optical and Quantum Electronics* **55**, 460 (2023).
- [12] G. Shukla, D. Yadav, P. Sharma, A. Kumar, and D. K. Mishra, Quantum sub-phase sensitivity of a mach-zehnder interferometer with the superposition of schrödinger's cat-like state with vacuum state as an input under product detection scheme, *Physics Open* **18**, 100200 (2024).
- [13] X.-W. Zheng, J.-C. Zheng, X.-F. Pan, and P. Li, Quantum-enhanced sensing of bosonic modes with cat states, *Phys. Rev. A* **112**, 032612 (2025).
- [14] R. Demkowicz-Dobrzanski, M. Jarzyna, and J. Kolodnyski, Chapter four - quantum limits in optical interferometry (Elsevier, 2015) pp. 345 – 435.
- [15] M. D. Lang and C. M. Caves, Optimal quantum-enhanced interferometry using a laser power source, *Phys. Rev. Lett.* **111**, 173601 (2013).
- [16] M. D. Lang and C. M. Caves, Optimal quantum-enhanced interferometry, *Phys. Rev. A* **90**, 025802 (2014).
- [17] C. W. Helstrom, *Quantum detection and estimation theory* (Academic Press, New York, 1976) p. 309.
- [18] M. A. Taylor, J. Janousek, V. Daria, J. Knittel, B. Hage, H.-A. Bachor, and W. P. Bowen, Biological measurement beyond the quantum limit, *Nature Photonics* **7**, 229 (2013).
- [19] H. Lotfipour, H. Sobhani, M. T. Dejjasand, and M. Sasani Ghamsari, Application of quantum imaging in biology, *Biomedical Optics Express* **16**, 3349 (2025).
- [20] P. T. Grochowski and R. Filip, Optimal phase-insensitive force sensing with non-gaussian states, *Phys. Rev. Lett.* **135**, 230802 (2025).
- [21] I. Ivanovic, How to differentiate between non-orthogonal states, *Physics Letters A* **123**, 257 (1987).
- [22] S. J. van Enk, Unambiguous state discrimination of coherent states with linear optics: Application to quantum cryptography, *Phys. Rev. A* **66**, 042313 (2002).
- [23] J. S. Sidhu, M. S. Bullock, S. Guha, and C. Lupo, Linear optics and photodetection achieve near-optimal unambiguous coherent state discrimination, *Quantum* **7**, 1025 (2023).
- [24] V. Dodonov, I. Malkin, and V. Man'Ko, Even and odd coherent states and excitations of a singular oscillator, *Physica* **72**, 597 (1974).
- [25] T. C. Ralph, A. Gilchrist, G. J. Milburn, W. J. Munro, and S. Glancy, Quantum computation with optical coherent states, *Physical Review A* **68**, 042319 (2003).
- [26] T. C. Ralph, A. Hayes, and A. Gilchrist, Loss-tolerant optical qubits, *Physical review letters* **95**, 100501 (2005).
- [27] G.-Y. Xiang, T. C. Ralph, A. P. Lund, N. Walk, and G. J. Pryde, Heralded noiseless linear amplification and distillation of entanglement, *Nature Photonics* **4**, 316 (2010).
- [28] B. P. Lanyon, M. Barbieri, M. P. Almeida, T. Jennewein, T. C. Ralph, K. J. Resch, G. J. Pryde, J. L. O'brien, A. Gilchrist, and A. G. White, Simplifying quantum logic using higher-dimensional hilbert spaces, *Nature Physics* **5**, 134 (2009).
- [29] A. P. Lund, T. C. Ralph, and H. L. Haselgrove, Fault-tolerant linear optical quantum computing with small-amplitude coherent states, *Physical review letters* **100**, 030503 (2008).
- [30] H.-L. Yin and Z.-B. Chen, Coherent-state-based twin-field quantum key distribution, *Scientific reports* **9**, 14918 (2019).
- [31] D. S. Schlegel, F. Minganti, and V. Savona, Quantum error correction using squeezed schrödinger cat states, *Phys. Rev. A* **106**, 022431 (2022).
- [32] V. Gorshenin, Using schrödinger cat quantum state for detection of a given phase shift, *Laser Physics Letters* **21**, 065201 (2024).
- [33] V. Gorshenin and F. Y. Khalili, Using non-gaussian quantum states for detection of a given phase shift, *Journal of the Optical Society of America B* **42**, 1448 (2025).
- [34] U. Leonhardt and H. Paul, Realistic optical homodyne measurements and quasiprobability distributions, *Phys. Rev. A* **48**, 4598 (1993).
- [35] R. Filip, Gaussian quantum adaptation of non-gaussian states for a lossy channel, *Phys. Rev. A* **87**, 042308 (2013).
- [36] H. Le Jeannic, A. Cavaillès, K. Huang, R. Filip, and J. Laurat, Slowing quantum decoherence by squeezing in phase space, *Phys. Rev. Lett.* **120**, 073603 (2018).
- [37] B. Nugmanov, N. Zunikov, and F. Y. Khalili, Robustness of negativity of the wigner function to dissipation (2022), [arXiv:2201.03257 \[quant-ph\]](https://arxiv.org/abs/2201.03257).
- [38] H. Le Jeannic, A. Cavaillès, K. Huang, R. Filip, and J. Laurat, Slowing quantum decoherence by squeezing in phase space, *Phys. Rev. Lett.* **120**, 073603 (2018).
- [39] C. W. Helstrom, Detection theory and quantum mechanics, *Information and Control* **10**, 254 (1967).
- [40] L. Stasi, G. Gras, R. Berrazouane, M. Perrenoud, H. Zbinden, and F. Bussièrès, Fast high-efficiency photon-number-resolving parallel superconducting nanowire single-photon detector, *Phys. Rev. Appl.* **19**, 064041 (2023).
- [41] A. E. Lita, A. J. Miller, and S. W. Nam, Counting near-infrared single-photons with 95% efficiency, *Optics express* **16**, 3032 (2008).
- [42] D. Fukuda, G. Fujii, T. Numata, K. Amemiya, A. Yoshizawa, H. Tsuchida, H. Fujino, H. Ishii, T. Itatani, S. Inoue, and T. Zama, Titanium-based transition-edge photon number resolving detector with 98% detection efficiency with index-matched small-gap fiber coupling, *Opt. Express* **19**, 870 (2011).
- [43] T. Gerrits, B. Calkins, N. Tomlin, A. E. Lita, A. Migdall, R. Mirin, and S. W. Nam, Extending single-photon optimized superconducting transition edge sensors beyond the single-photon counting regime, *Opt. Express* **20**, 23798 (2012).
- [44] A. Ourjoumtsev, R. Tualle-Brouri, J. Laurat, and P. Grangier, Generating optical schrödinger kittens for quantum information processing, *Science* **312**, 83 (2006).
- [45] K. Huang, H. Le Jeannic, J. Ruauel, V. B. Verma, M. D. Shaw, F. Marsili, S. W. Nam, E. Wu, H. Zeng, Y.-C. Jeong, R. Filip, O. Morin, and J. Laurat, Optical synthesis of large-amplitude squeezed coherent-state superpositions with minimal resources, *Phys. Rev. Lett.* **115**, 023602 (2015).

- [46] D. V. Sychev, A. E. Ulanov, A. A. Pushkina, M. W. Richards, I. A. Fedorov, and A. I. Lvovsky, Enlargement of optical schrödinger's cat states, *Nature Photonics* **11**, 379 (2017).
- [47] D. A. Kuts, M. S. Podoshvedov, B. A. Nguyen, and S. A. Podoshvedov, Realistic conversion of single-mode squeezed vacuum state to large-amplitude high-fidelity schrödinger cat states by inefficient photon number resolving detection, *Physica Scripta* **97**, 115002 (2022).
- [48] M. S. Podoshvedov, S. A. Podoshvedov, and S. P. Kulik, Algorithm of quantum engineering of large-amplitude high-fidelity schrödinger cat states, *Scientific Reports* **13**, 3965 (2023).
- [49] A. Inoue, T. Kashiwazaki, T. Yamashima, N. Takanashi, T. Kazama, K. Enbutsu, K. Watanabe, T. Umeki, M. Endo, and A. Furusawa, Toward a multi-core ultra-fast optical quantum processor: 43-ghz bandwidth real-time amplitude measurement of 5-db squeezed light using modularized optical parametric amplifier with 5g technology, *Applied Physics Letters* **122** (2023).
- [50] T. S. Iskhakov, V. C. Usenko, U. L. Andersen, R. Filip, M. V. Chekhova, and G. Leuchs, Heralded source of bright multi-mode mesoscopic sub-poissonian light, *Optics letters* **41**, 2149 (2016).
- [51] G. Frascella, S. Agne, F. Y. Khalili, and M. V. Chekhova, Overcoming detection loss and noise in squeezing-based optical sensing, *npj Quantum Information* **7**, 72 (2021).
- [52] Code used for numerical calculations, <https://github.com/valentien/ng-interferometry-sq-2026> (2026).
- [53] DLMF, *NIST Digital Library of Mathematical Functions*, <https://dlmf.nist.gov/>, Release 1.2.4 of 2025-03-15, f. W. J. Olver, A. B. Olde Daalhuis, D. W. Lozier, B. I. Schneider, R. F. Boisvert, C. W. Clark, B. R. Miller, B. V. Saunders, H. S. Cohl, and M. A. McClain, eds.